Coherent optical creation of a single molecule

Yichao Yu,[1,2,3,*] Kenneth Wang,[1,2,3] Jonathan D. Hood,[4] Lewis R. B. Picard,[1,2,3] Jessie T. Zhang,[1,2,3] William B. Cairncross,[2,1,3] Jeremy M. Hutson,[5] Till Rosenband,[1] and Kang-Kuen Ni[2,1,3,†]

[1] *Department of Physics, Harvard University, Cambridge, Massachusetts 02138, USA*
[2] *Department of Chemistry and Chemical Biology, Harvard University, Cambridge, Massachusetts 02138, USA*
[3] *Harvard-MIT Center for Ultracold Atoms, Cambridge, Massachusetts 02138, USA*
[4] *Department of Chemistry, Purdue University, West Lafayette, Indianna, 47906, USA*
[5] *Joint Quantum Centre Durham-Newcastle, Department of Chemistry, Durham University, Durham, DH1 3LE, United Kingdom*

(Dated: December 3, 2020)

We report on coherent association of atoms into a single weakly bound NaCs molecule in an optical tweezer through an optical Raman transition. The Raman scheme uses a deeply bound electronic excited intermediate state to achieve a large transition dipole moment while reducing photon scattering. Starting from two atoms in their relative motional ground state, we achieve an optical transfer efficiency of 69%. The molecules have a binding energy of 770.1969(2) MHz at 8.83(2) G and are created with higher than 60% probability in the motional ground state. This technique does not rely on Feshbach resonances or narrow excited-state lines and may allow a wide range of molecular species to be assembled atom-by-atom.

Diverse species of fully quantum controlled ultracold molecules are desired for a wide variety of applications including precision measurements [1–6], quantum simulations [7–10], quantum information processing [11–14], and studies of ultracold chemistry [15–18]. While many innovative approaches demonstrated in the last few years have directly cooled different species of diatomic or polyatomic molecules below 1 mK [19–24], the highest phase-space-density gas [25] and the coldest individual molecules [26, 27] have been achieved through the association of ultracold atoms.

Molecular association of ultracold atoms takes advantage of the cooling and trapping techniques that have been developed for atoms. Associating atoms into deeply bound molecules is challenging because of the small wavefunction overlap between the free-atom and molecular states and the release of a large amount of binding energy. A widely used method of overcoming these challenges is to associate atom pairs into weakly bound molecules first, and then transfer the molecules from this single internal state to a desired rovibrational and electronic state, releasing the binding energy by stimulated emission [1, 28–35]. So far, molecular association has generally been achieved by magnetoassociation using a magnetic Feshbach scattering resonance. Exceptions include Sr_2, where narrow linewidth (~ 20 kHz) excited states are available and optical association can be driven coherently [36, 37], and $^{87}Rb^{85}Rb$, where there are molecular states bound by $1-2$ MHz [27]. With these requirements, molecules involving non-magnetic atoms or atoms without narrow intercombination lines remain difficult to associate.

Here, we demonstrate coherent association of an atom pair to a weakly bound molecule by two-photon optical Raman transfer via an electronic excited state, schematically shown in Fig. 1a. The scheme does not rely on a Feshbach resonance, molecular states bound by a few MHz, or a narrow excited state. The resulting single molecule is in a well-defined internal quantum state and predominantly in its motional ground state. A vibrational state of the electronic excited state $c^3\Sigma^+(\Omega = 1)$ is used as the intermediate state in the Raman scheme, and is chosen to minimize photon scattering during Raman Rabi oscillations. To reduce photon scattering and sensitivity to laser intensity noise further, we choose the initial and final states to balance the two Rabi frequencies as much as possible. This system-independent approach creates molecules atom-by-atom with full quantum state control.

The essence of an optical Raman transfer can be illustrated using a three-level system shown in Fig. 1a, where the initial atomic state and the target weakly bound molecular state are coupled to an intermediate state by two lasers with Rabi frequencies, Ω_a and Ω_m, with one-photon detuning Δ, and two-photon detuning, δ. The transfer Raman Rabi Rate is given by $\Omega_a\Omega_m/2\Delta$ [38]. Unlike Raman transitions in atoms, the two Rabi frequencies are greatly imbalanced due to the small wavefunction overlap between the atomic state and the intermediate state, and therefore the scattering is predominantly from the target molecular state. Furthermore, the energy difference between the atomic state and target molecular state is small (< 1 GHz) compared to the single-photon detuning, Δ, so the target molecular state can scatter off both beams roughly equally. Thus, the scattering rate is given by $\Gamma_e\Omega_m^2/2\Delta^2$, where Γ_e is the excited-state linewidth [39]. The ratio between the Raman Rabi frequency and the scattering rate is therefore $\Omega_a/\Omega_m \times \Delta/\Gamma_e$. To ensure a coherent process, a detuning as large as possible, while maintaining a realistic Raman Rabi frequency, is preferred.

Earlier experiments used weakly bound excited states as the intermediate state in the Raman transition to en-

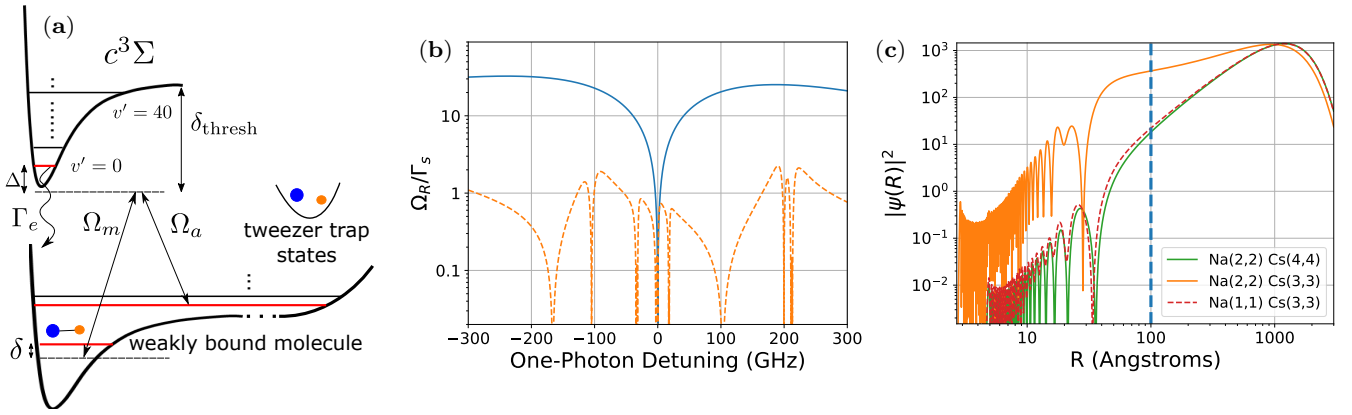

FIG. 1. Optical creation of single molecule from single atoms in tweezer. (a) Schematic of the optical transition from an atom pair to a weakly bound molecule. The initial state is the relative motional ground state between the two atoms and the final state is the first molecular bound state. The transition is driven by a pair of laser frequencies matching the binding energy of the molecule. The lasers are detuned from an excited molecular state in the $c^3\Sigma$ potential by Δ in order to suppress scattering during the transfer. (b) Comparison between using a weakly bound and a deeply bound excited state as intermediate state for the Raman transition. The deeply bound excited state (blue lines $v' = 0$) has a smaller Raman Rabi frequency (Ω_R) compared to the weakly bound excited state (orange lines $v' = 40$) at a most detuning. However, the scattering rate (Γ_s) is also much lower, which results in a larger ratio of Raman Rabi frequency to scattering rate. (c) Enhancement of the short-range wavefunction. The large scattering length for the $\text{Na}(2,2), \text{Cs}(3,3)$ state creates an interaction shift comparable to the axial trapping frequency. This causes a significant change in the relative wavefunction, especially at short internuclear distance (R). Compared to other spin states with weaker interaction, the wavefunction at short distance ($R < 100$ Å, left of the dashed line) is significantly enhanced.

sure a large Raman Rabi frequency [40, 41]. However, a complete picture must include both the many vibrational levels of the excited electronic state and the atomic continuum. The total scattering rate and Raman Rabi rate become a sum of the scattering rates and Raman Rabi rates over all possible intermediate states. Since there is large overlap between the target molecular state and weakly bound excited states, using states that are closer to the dissociation threshold as the intermediate state results in a large scattering rate. This scattering is approximately proportional to $1/\delta^2_{\text{thresh}}$, where δ_{thresh} is the detuning from the dissociation threshold, and thus can be made smaller by using deeply bound vibrational states as the intermediate state.

To find the optimal intermediate state, we perform a calculation of the Raman Rabi frequency Ω_R and scattering rate Γ_s at different detunings from the atomic threshold taking into account of all states of 8 excited molecular potentials [42–46] and the continuum [47]. This calculation shows that Ω_R/Γ_s can be made larger for more deeply bound states compared to weakly bound states at a cost of a smaller Ω_R, as shown in Fig. 1b; see Supplementary Material for details. As a result, we choose the $v' = 0$ level of $c^3\Sigma^+(\Omega = 1)$ as the closest intermediate state to drive the Raman transition.

In addition to the intermediate state, choosing an initial and a final state for a large ratio Ω_a/Ω_m maximizes Ω_R at a given detuning. Furthermore, a larger ratio also relaxes the intensity stability requirement for the Raman lasers, because this is also the ratio between Ω_R and the AC Stark shift of the molecular state, $\Omega_m^2/2\Delta$ [48]. Due to the small extent of the intermediate-state wavefunction compared to that of the trapped atoms, Ω_a is approximately proportional to the amplitude of the relative atomic wavefunction at short distance, within the range of the molecular potential. To increase this amplitude, one can increase the external confinement of atom pairs. Using a harmonic approximation, the short-range amplitude is proportional to $\omega_{\text{trap}}^{3/4}$ or $P^{3/8}$, where ω_{trap} is the trap frequency and P is the optical power in the tweezer trap [49]. However, additional power may not always be available, and will also lead to additional undesired scattering. Alternatively, one can choose an atomic pair state with a large scattering length (positive or negative). For such states, the amplitude of the relative atomic wavefunction is substantially enhanced at short range, as shown in Fig. 1c. For our system of Na and Cs atoms, we choose a spin-state combination $|{\uparrow_{\text{Na}}}{\downarrow_{\text{Cs}}}\rangle \equiv |f = 2, m_f = 2\rangle_{\text{Na}} |f = 3, m_f = 3\rangle_{\text{Cs}}$ that has a large and negative scattering length of $a({\uparrow_{\text{Na}}}{\downarrow_{\text{Cs}}}) \approx -700 a_0$ [50]. All other stable spin combinations give smaller scattering lengths ($< 50\ a_0$).

To identify a suitable target molecular state, we carry out coupled-channel calculations of the near-threshold bound states, as described in the Supplemental Material. Choosing a bound state with similar spin character to the atomic state minimizes the sensitivity of the transition frequency to magnetic field. A suitable state

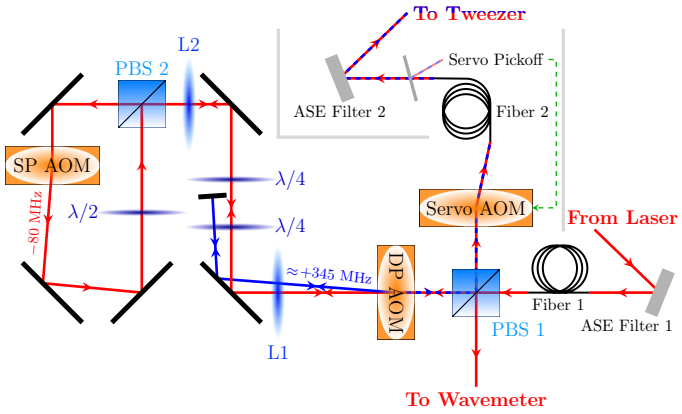

FIG. 2. Beampath for generating the frequency for Raman transition in the tweezer. (Some mirrors and other optics used for alignment are not included.) The two ASE filters before and after the fibers are also shown. The red beam path is the 0-th order of the double pass (DP) AOM which is used for the tweezer. When the double-pass (DP) AOM is turned on, some power is redirected to the first order (blue beam path) which generates the required frequency different to drive the Raman transition. The two frequencies are recombined on the DP AOM. The 0-th order light is shifted by another single pass (SP) AOM running on a different frequency before recombining. Without this AOM, the leak light from the DP AOM will be at the same frequency as the 0-th order light which can cause a significant power fluctuation due to interference. The experiment typically start with the SP AOM on and the DP AOM off. When driving the Raman transition, the powers on both AOMs are ramped simultaneously to achieve the desired power at both frequencies.

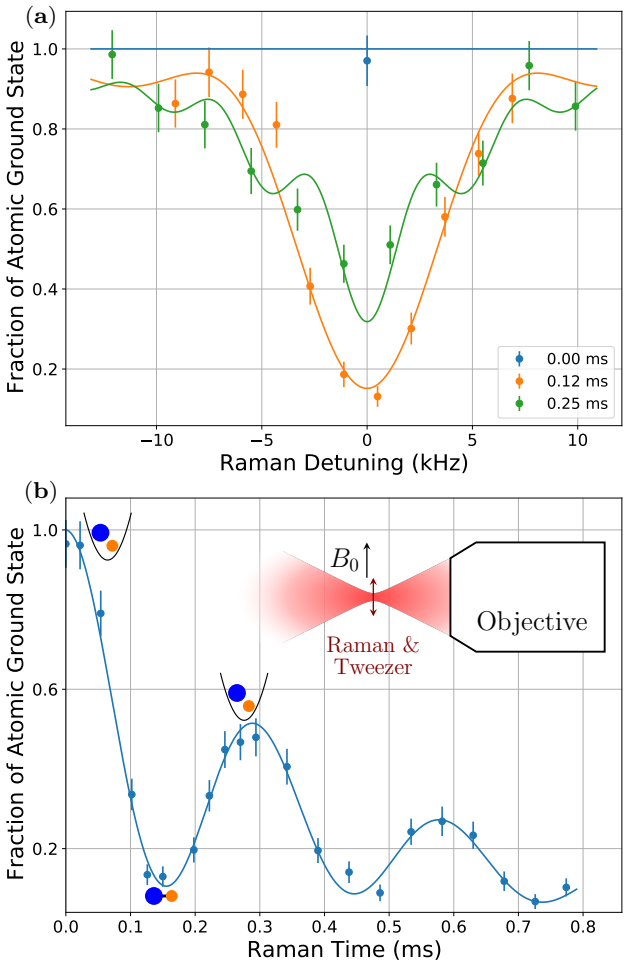

FIG. 3. (a) Raman detuning scans at different times showing the resonance frequency. (b) Raman pulse-time scan on resonance. A decaying Rabi oscillation can be observed, proving the coherence of the Raman transfer process. This is fitted together with (a) to a model of the Raman transition including loss of the atom and molecule state and is used to determine both the Raman Rabi frequency and the loss rates. Inset: Geometry and polarization of trap and Raman beam relative to the bias magnetic field. The tweezer and Raman beam is focused through an objective to a waist of 0.9 μm, which defines the location of the atoms and molecule. We use a bias magnetic field $B_0 = 8.83(2)$ G along the tweezer polarization to define the quantization axis. As a result, the atoms experience predominantly π polarization from the tweezer.

with this character is predicted about 763 MHz below the $|\uparrow_{\mathrm{Na}}\downarrow_{\mathrm{Cs}}\rangle$ threshold. The ratio Ω_a/Ω_m increases to about 0.013 when starting from atoms in the $|\uparrow_{\mathrm{Na}}\downarrow_{\mathrm{Cs}}\rangle$ hyperfine combination. Compared to 0.003 with the other combinations, this relaxes the intensity stability requirement to the percent level.

Experimentally, we first prepare two atoms in a well-defined external and internal quantum state using techniques developed previously [51–53]. In brief, the experimental cycle begins by stochastically loading a single ^{23}Na atom and a single ^{133}Cs atom into separate optical tweezers. The atoms are initially imaged to distinguish between loading of two atoms, one atom (Na or Cs), or no atom to be able to post-select from the experimental results based on the initial loading condition. After imaging, we turn on a 8.83(2) G magnetic field to define the quantization axis for the state preparation and molecule formation steps. Raman sideband cooling is then applied to prepare both atoms simultaneously in the 3-dimensional motional ground state of their optical tweezers. After cooling, the Na and Cs atoms are in the spin state $|\uparrow_{\mathrm{Na}}\uparrow_{\mathrm{Cs}}\rangle \equiv |f=2, m_f=2\rangle_{\mathrm{Na}} |f=4, m_f=4\rangle_{\mathrm{Cs}}$, which has a small scattering length. The weak two-atom interaction allows the merging of the two tweezers to be done with minimum pertubation so that they remain in the motional ground state.

Next, we drive the atoms into spin combination $|\uparrow_{\mathrm{Na}}\downarrow_{\mathrm{Cs}}\rangle$, which has large scattering length, by performing a Cs spin flip while taking into account the −30.7 kHz interaction shift [50]. We use this as the initial atomic state for Raman transfer. This spin flip selectively transfers atoms in the relative motional ground state, removing any background from atoms in excited motional states [54]. For the experiment reported here, 31% of our

initial two-atom population is transferred.

To perform the Raman transfer of an atom pair to the target weakly bound molecular state, we use the tweezer beam itself as the Raman beams by turning on two frequencies in the tweezer during the Raman pulse using an acousto-optic modulator, as shown in Fig. 2. The dual use of the tweezer beam not only eliminates additional scattering sources or undesired laser frequencies, but also allows a tight focus to maximize the Raman Rabi frequency and minimize the transfer time. Furthermore, we use two Bragg gratings, each with a linewidth (FWHM) of 50 GHz, to filter the laser spectrum. As shown in Fig. 2, we place one filter directly after the laser, which is a fiber amplifer seeded with a 1037 nm external cavity diode laser. We place the second filter as close to the microscope objective as possible. We observe a reduction of the scattering rate by a factor of 2 due to suppression of the broadband amplified spontaneous emission (ASE) from the laser that couples to other excited states. After the total tweezer power is set to the desired value, we smoothly ramp down the power of one frequency in the tweezer while simultaneously ramping up the power of the other frequency so that the total tweezer power remains unchanged. Both frequencies are kept on for a specified duration before the process is reversed and the tweezer returns to a single frequency.

We choose the tweezer frequency to be 288560 GHz which is far detuned (by $\approx$151 GHz) from the $v' = 0$ line. Guided by the coupled-channel calculations, we locate the Raman resonance for the atoms-to-molecule transition at 770.57150(9) MHz with about 3.75 mW tweezer power focused down to a waist of 0.9 μm, as shown in Fig. 3a. The molecular state is dark to the imaging step, so successful transfer of the atoms to the molecular state is detected as loss of atoms. We observe a Fourier-limited linewidth, which is evidence of a coherent transfer. In order to verify the coherence of the transfer directly, we fix the two-photon detuning on resonance and scan the pulse time. Fig. 3b shows the observed coherent Rabi oscillation between the atomic and molecular states. Fitting the data with a decaying Rabi oscillation suggests that 69 % of atoms initially in the motional ground state are transferred into the molecular state after a π pulse. This transfer efficiency is limited mainly by the molecular lifetime, which can be measured directly by preparing the molecule with a π pulse and then using a second π pulse to dissociate the molecule back to atoms after a variable wait time. The result in Fig. 4a shows a molecular lifetime of 0.199(9) ms consistent with the decay of the Rabi oscillation. We obtain the Raman Rabi frequency by fitting our measurements to a model that includes a Raman Rabi frequency and a finite lifetime for the molecular state, as shown in Fig. 3a and b. We account for the small effect of atomic state loss by measuring the one-body and two-body lifetime of the atoms directly without turning on the second frequency, as shown in Fig. 4b.

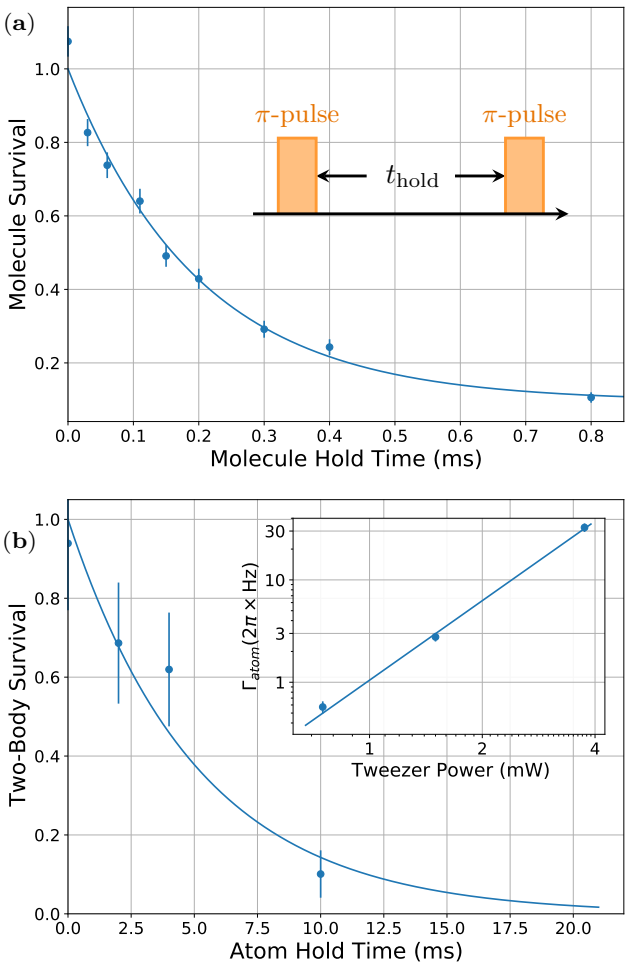

FIG. 4. (a) Direct measurement of molecule lifetime in a trap of depth 3.75 mW. Molecule survival is detected by dissociating back to atoms using a second Raman transition. The lifetime is consistent with the 0.199(9) ms measured from the Raman transition data. Inset: pulse sequence for the lifetime measurement. (b) Two-body atom lifetime of 5(1) ms in a trap of depth 3.75 mW caused by off-resonance photoassociation. This is used to improve the fitting of the Raman transfer data. Inset: Atomic scattering rate scales as $P_{\mathrm{tweezer}}^{2.58} \times 2\pi \times 29.3(17)$ mHz/mW$^{2.58}$ on a log-log scale; this is consistent with a two-photon scattering process. We have not measured a clear dependency of the loss rate on the tweezer detuning.

The fit including all these effects gives a Raman Rabi frequency of $2\pi \times 3.28(4)$ kHz.

The efficiency of the transfer is lower than expected because we found the ratio of the molecular scattering rate (i.e. inverse of lifetime) to the Rabi frequency is 10 times larger than predicted. This discrepancy can arise from the $v' = 0$ excited state, if the ratio Ω_m/Ω_a or Γ_e are larger than expected. Additionally, coupling to other excited states can add an offset to both the Raman Rabi frequency and the scattering rate and thus affect their

ratio.

In order to verify whether any one of these sources are the origin of the reduced transfer efficiency, we measured the properties of the Raman resonance as a function of the tweezer power and single-photon detuning. These dependencies allow us to experimentally determine the Rabi frequencies, Ω_a, Ω_m and how much of the scattering, Stark shift, or Raman Rabi frequency comes from the $v' = 0$ intermediate state.

P (mW)	0.75	1.5	3.75
f_{PA0} (GHz)	288711.8		
a ($2\pi \times$ MHz)	770.20452(6)	770.2081(1)	770.1943(3)
b ($4\pi^2 \times$ MHz $\cdot$ GHz)	$-12.46(2)$	$-24.44(3)$	$-60.66(8)$
c ($2\pi \times$ kHz)	0.29(2)	0.63(4)	2.4(2)
d ($4\pi^2 \times$ MHz $\cdot$ GHz)	0.115(4)	0.275(6)	0.95(3)

TABLE I. Fitting results for Fig. 5(a,b).

To determine Ω_m and Ω_a, we measure the change in resonance frequency and Raman Rabi frequency as a function of the tweezer detuning. For both these quantities, we observe a $1/\Delta$ component and a constant background in the experimentally explored region, as shown in Fig. 5a, b. The background is caused by coupling to other excited states that are further away in energy. The $1/\Delta$ component, however, is due to the coupling to the $v' = 0$ intermediate state. Combining the fit coefficients, summarized in Table I, for the $1/\Delta$ component, we can extract Ω_m and Ω_a.

We perform the experiment at various tweezer powers to extract the power dependence of Ω_m and Ω_a, as shown in Fig. 5c. Ω_m scales with $P^{0.5}$ as expected, and we obtain a fit value of $2\pi \times 180.87(7)$ MHz$/\sqrt{\mathrm{mW}}$. This number is within 40 % of the value $2\pi \times 296$ MHz$/\sqrt{\mathrm{mW}}$ calculated from theory. The scaling of Ω_a differs from $P^{0.5}$, which is the expected scaling from the laser intensity, due to the change in the atomic wavefunction caused by tighter confinement at higher power. For weakly interacting particles, Ω_a scales as $P^{3/8}$. However, due to the strong interaction between the two atoms in the $|{\uparrow_{\mathrm{Na}}}{\downarrow_{\mathrm{Cs}}}\rangle$ state, this approximation breaks down. Instead, coupled-channel calculations show that the scaling is very well approximated by $P^{0.29}$ within the range of confinement in our experiment. Thus, Ω_a scales as $P^{0.79}$, which fits well to our experimental result. The fit value is $2\pi \times 1.85(3)$ MHz/P$^{0.79}$. At 3.75 mW tweezer power, we measured $\Omega_m = 2\pi \times 348.3(3)$ MHz and $\Omega_a = 2\pi \times 5.5(2)$ MHz, resulting in a Ω_m/Ω_a ratio of about 63, which is close to the theory prediction of 77.7 (Table II). Therefore, the matrix element ratio is not the cause of our lower than expected transfer efficiency. Furthermore, we independently measure the natural linewidth of the $v' = 0$ excited state to be no larger than 50 MHz using photoassociation (PA) spectroscopy, which cannot explain the excess scattering either.

	Experiment	Theory
Ω_R	$2\pi \times 3.28(4)$ kHz	$2\pi \times 15.3$ kHz
Γ_s	$2\pi \times 0.80(4)$ kHz	$2\pi \times 533$ Hz
Ω_m	$2\pi \times 348.3(3)$ MHz	$2\pi \times 573$ MHz
Ω_a	$2\pi \times 5.5(2)$ MHz	$2\pi \times 7.37$ MHz
Ω_m/Ω_a	63(3)	77.7

TABLE II. Comparison between theory and experiment of $\Omega_R, \Gamma_s, \Omega_m, \Omega_a$. Ω_R and Γ_s are reported at 151 GHz detuned from the $v' = 0$ state. All numbers are reported at 3.75 mW tweezer power.

We now consider the background effects from other states with larger single-photon detuning. In the Raman Rabi frequency fit, the fitted background is of opposite sign from the Raman Rabi frequency for single-photon detunings red of the $v' = 0$ transition. Thus, this background reduces the Raman Rabi frequency by about 30 % at the current detuning. However, this difference is not enough to explain the discrapancy of more than a factor of 10 present in the experiment. Due to the change in sign of the Raman Rabi frequency as a function of detuning when crossing a resonance, the same background will increase the Raman Rabi frequency for positive detunings from the $v' = 0$ transition. Unfortunately, we observe additional nearby excited states belonging to a different electronically excited state at higher frequencies which prevent the blue side of the transition from being be usable for the Raman transition.

These results suggest that the decoherence or loss we observe during the Raman transition comes from either a higher background scattering rate of an unknown source or a different intrinsic or technical source for which we have not accounted for. We observe a decrease in the coherence time by a factor of 2 without the ASE filters. This suggests the spectral purity of the laser is a significant source of scattering, but does not explain the full amount. Other sources that can contribute to the decoherence include the stability of the tweezer power and the magnetic field. Based on the ratio of the Raman Rabi frequency to light shift, shown in Fig. 5c, the requirement on the tweezer power stability is 0.8% at 3.75 mW. We stabilize the power to 0.1%, so this should not be a major source of decoherence. Similarly, we measured a Zeeman shift of 42.2(2) kHz/G which does not cause significant decoherence from the measured magnetic field fluctuation of ~ 1.5 mG.

The scattering rate of the molecule also depends on the tweezer power and detuning, and becomes smaller when the power is lowered. At 0.75 mW tweezer power, we observe a molecule lifetime as long as 1 ms. Since the technical noise that can lead to decoherence is not fully characterized in our experiment, we are unable to further identify the sources of the measured scattering rate based on our measured detuning and power dependencies.

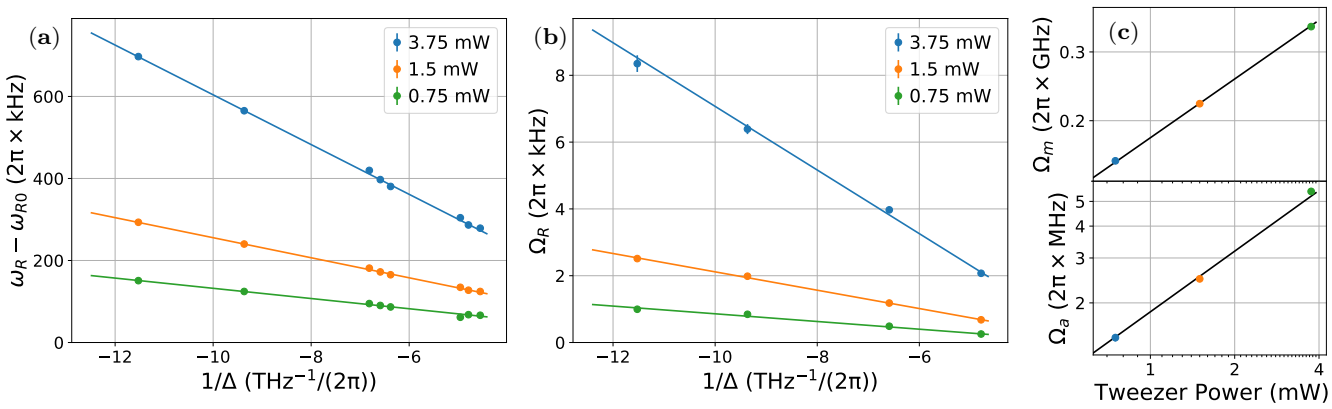

FIG. 5. Raman transition parameters as a function of tweezer and Raman power and detuning. (a) The Raman resonance fitted to $a_P + b_P/\Delta$, where a_P and $b_P = (\Omega_a^2 - \Omega_m^2)/2$ are tweezer power dependent background and $v' = 0$ contribution to the light shift, $\Delta \equiv 2\pi \times (f_{\mathrm{PA0}} - f_{\mathrm{tweezer}})$ is the detuning from the PA resonance frequency f_{PA0}. The a_Ps are fitted to a model including linear and small quadratic light shift to obtain the Raman resonance frequency at zero tweezer power to be $\omega_{R0} = 2\pi \times 770.1969(2)$ MHz. (b) Raman Rabi frequency (Ω_R) fitted to $c_P + d_P/\Delta$, where c_P and $d_P = \Omega_a\Omega_m/2$ are tweezer power dependent background and $v' = 0$ contribution. The detuning is calculated using the PA frequency fitted in (a). The c_Ps and d_Ps are proportional to $P^{1.29}$ and the fit gives $c_P/P^{1.29} = -2\pi \times 0.41(2)$ kHz/mW$^{1.29}$ and $d_P/P^{1.29} = -4\pi^2 \times 167(2)$ kHz $\cdot$ GHz/mW$^{1.29}$. The fitting results for (a) and (b) are shown in Table I. (c) Tweezer power dependency of Ω_m (top) and Ω_a (bottom) calculated from b_P and d_P on a log-log scale showing the $P^{0.5}$ scaling of Ω_m and the $P^{0.79}$ scaling of Ω_a.

Lastly, to confirm that the excess scattering does not come from the atomic state, we measure the two-body scattering rate without turning on the second frequency, as shown in Fig. 4b inset. The scattering rate scales as $P^{2.58}$, which is inconsistent with a single-photon scattering process. We have not been able to observe a dependency on the detuning in order to verify whether the scattering process is related to the $v' = 0$ state, but the power scaling strongly suggests the existence of an unknown two-photon process. Nevertheless, the absolute scattering rate from the atomic state is much lower than the total scattering rate and is not the limiting factor in this experiment.

In conclusion, we have formed a weakly bound NaCs molecule in an optical tweezer by optical Raman transfer. A theoretical investigation including 8 excited state potentials, the excited atomic continuum, and coupled-channel ground state wavefunctions indicated better transfer efficiency using a deeply bound intermediate state and the $|{\uparrow_{\mathrm{Na}}}{\downarrow_{\mathrm{Cs}}}\rangle$ spin state as the initial and final states. Using these theoretical insights, we located the weakly bound state and coherently associated the atoms into a weakly bound molecule. Currently, Our transfer efficiency is limited by an unknown scattering source resulting in measured scattering rates over 10 times larger than theoretical predictions. Despite this limitation, the transfer efficiency may be further improved by increasing the ratio of the up-leg to down-leg Rabi frequency Ω_a/Ω_m, for example by driving to more deeply bound states.

Our technique can be applied to form a more diverse set of molecular species, since it does not rely on a magnetic Feshbach resonance, states bound by a few MHz, or a narrow excited state. The formation of a weakly bound molecule is a key step in forming rovibrational ground state molecules. By scaling up to many optical tweezers[55–58], large arrays with arbitrary geometry of highly controlled molecules can be achieved.

We would like to thank Rosario Gonzalez-Ferez, Olivier Dulieu, Bo Gao, and Paul Julienne acknowledge getting TDM for discussion. This work is supported by the NSF (PHY-1806595), the AFOSR (FA9550-19-1-0089), ARO DURIP (W911NF1810194) and the Arnold and Mabel Beckman foundation. J. T. Z. is supported by a National Defense Science and Engineering Graduate Fellowship. W. C. is supported by a Max Planck-Harvard Research Center for Quantum Optics fellowship. K. W. is supported by an NSF GRFP fellowship. J. M. H. is supported by the U.K. Engineering and Physical Sciences Research Council (EPSRC) Grants No. EP/N007085/1, EP/P008275/1 and EP/P01058X/1.

* yichaoyu@g.harvard.edu
† ni@chemistry.harvard.edu

[1] S. S. Kondov, C.-H. Lee, K. H. Leung, C. Liedl, I. Majewska, R. Moszynski, and T. Zelevinsky, Nature Physics **15**, 1118–1122 (2019).
[2] I. Kozyryev and N. R. Hutzler, Physical Review Letters **119**, 133002 (2017), publisher: American Physical Society.

[3] V. V. Flambaum and V. A. Dzuba, Phys. Rev. A **101**, 042504 (2020).
[4] V. Andreev, D. G. Ang, D. DeMille, J. M. Doyle, G. Gabrielse, J. Haefner, N. R. Hutzler, Z. Lasner, C. Meisenhelder, B. R. O'Leary, C. D. Panda, A. D. West, E. P. West, X. Wu, and A. C. M. E. Collaboration, Nature **562**, 355 (2018).
[5] W. B. Cairncross, D. N. Gresh, M. Grau, K. C. Cossel, T. S. Roussy, Y. Ni, Y. Zhou, J. Ye, and E. A. Cornell, Phys. Rev. Lett. **119**, 153001 (2017).
[6] J. J. Hudson, D. M. Kara, I. J. Smallman, B. E. Sauer, M. R. Tarbutt, and E. A. Hinds, Nature **473**, 493 (2011).
[7] A. Micheli, G. Brennen, and P. Zoller, Nat. Phys. **2**, 341 (2006).
[8] N. Y. Yao, M. P. Zaletel, D. M. Stamper-Kurn, and A. Vishwanath, Nature Physics **14**, 405 (2018).
[9] M. L. Wall, K. R. A. Hazzard, and A. M. Rey, From atomic to mesoscale: The role of quantum coherence in systems of various complexities (World Scientific, 2015) Chap. Quantum magnetism with ultracold molecules.
[10] M. Wall, K. Maeda, and L. D. Carr, New Journal of Physics **17**, 025001 (2015).
[11] D. DeMille, Phys. Rev. Lett. **88**, 067901 (2002).
[12] K.-K. Ni, T. Rosenband, and D. D. Grimes, Chem. Sci. **9**, 6830 (2018).
[13] E. R. Hudson and W. C. Campbell, Phys. Rev. A **98**, 040302(R) (2018).
[14] Y. Lin, D. R. Leibrandt, D. Leibfried, and C.-W. Chou, Nature **581**, 273 (2020).
[15] N. Balakrishnan, J. Chem. Phys. **145**, 150901 (2016).
[16] M.-G. Hu, Y. Liu, D. D. Grimes, Y.-W. Lin, A. H. Gheorghe, R. Vexiau, N. Bouloufa-Maafa, O. Dulieu, T. Rosenband, and K.-K. Ni, Science **366**, 1111 (2019).
[17] Y. Segev, M. Pitzer, M. Karpov, N. Akerman, J. Narevicius, and E. Narevicius, Nature **572**, 189 (2019).
[18] T. de Jongh, M. Besemer, Q. Shuai, T. Karman, A. van der Avoird, G. C. Groenenboom, and S. Y. T. van de Meerakker, Science **368**, 626 (2020), https://science.sciencemag.org/content/368/6491/626.full.pdf.
[19] E. B. Norrgard, D. J. McCarron, M. H. Steinecker, M. R. Tarbutt, and D. DeMille, Phys. Rev. Lett. **116**, 063004 (2016).
[20] L. Anderegg, B. L. Augenbraun, Y. Bao, S. Burchesky, L. W. Cheuk, W. Ketterle, and J. M. Doyle, Nature Physics **14**, 890 (2018).
[21] D. Mitra, N. B. Vilas, C. Hallas, L. Anderegg, B. L. Augenbraun, L. Baum, C. Miller, S. Raval, and J. M. Doyle, Science **369**, 1366 (2020).
[22] S. Ding, Y. Wu, I. A. Finneran, J. J. Burau, and J. Ye, Phys. Rev. X **10**, 021049 (2020).
[23] D. J. McCarron, M. H. Steinecker, Y. Zhu, and D. DeMille, Phys. Rev. Lett. **121**, 013202 (2018).
[24] S. Truppe, H. J. Williams, M. Hambach, L. Caldwell, N. J. Fitch, E. A. Hinds, B. E. Sauer, and M. R. Tarbutt, Nature Physics **13**, 1173 (2017).
[25] L. De Marco, G. Valtolina, K. Matsuda, W. G. Tobias, J. P. Covey, and J. Ye, Science **363**, 853 (2019).
[26] J. T. Zhang, Y. Yu, W. B. Cairncross, K. Wang, L. R. B. Picard, J. D. Hood, Y.-W. Lin, J. M. Hutson, and K.-K. Ni, Phys. Rev. Lett. **124**, 253401 (2020).
[27] X. He, K. Wang, J. Zhuang, P. Xu, X. Gao, R. Guo, C. Sheng, M. Liu, J. Wang, J. Li, G. V. Shlyapnikov, and M. Zhan, Science **370**, 331 (2020).
[28] J. G. Danzl, E. Haller, M. Gustavsson, M. J. Mark, R. Hart, N. Bouloufa, O. Dulieu, H. Ritsch, and H.-C. Nägerl, Science **321**, 1062 (2008).
[29] K.-K. Ni, S. Ospelkaus, M. H. G. de Miranda, A. Pe'er, B. Neyenhuis, J. J. Zirbel, S. Kotochigova, P. S. Julienne, D. S. Jin, and J. Ye, Science **322**, 231 (2008).
[30] F. Lang, K. Winkler, C. Strauss, R. Grimm, and J. Hecker Denschlag, Phys. Rev. Lett. **101**, 133005 (2008).
[31] T. Takekoshi, L. Reichsöllner, A. Schindewolf, J. M. Hutson, C. R. Le Sueur, O. Dulieu, F. Ferlaino, R. Grimm, and H.-C. Nägerl, Phys. Rev. Lett. **113**, 205301 (2014).
[32] P. K. Molony, P. D. Gregory, Z. Ji, B. Lu, M. P. Köppinger, C. R. Le Sueur, C. L. Blackley, J. M. Hutson, and S. L. Cornish, Phys. Rev. Lett. **113**, 255301 (2014).
[33] J. W. Park, S. A. Will, and M. W. Zwierlein, Phys. Rev. Lett. **114**, 205302 (2015).
[34] M. Guo, B. Zhu, B. Lu, X. Ye, F. Wang, R. Vexiau, N. Bouloufa-Maafa, G. Quéméner, O. Dulieu, and D. Wang, Phys. Rev. Lett. **116**, 205303 (2016).
[35] K. K. Voges, P. Gersema, M. Meyer zum Alten Borgloh, T. A. Schulze, T. Hartmann, A. Zenesini, and S. Ospelkaus, Phys. Rev. Lett. **125**, 083401 (2020).
[36] G. Reinaudi, C. B. Osborn, M. McDonald, S. Kotochigova, and T. Zelevinsky, Phys. Rev. Lett. **109**, 115303 (2012).
[37] S. Stellmer, B. Pasquiou, R. Grimm, and F. Schreck, Phys. Rev. Lett. **109**, 115302 (2012).
[38] D. J. Wineland, M. Barrett, J. Britton, J. Chiaverini, B. DeMarco, W. M. Itano, B. Jelenković, C. Langer, D. Leibfried, V. Meyer, T. Rosenband, and T. Schätz, Philosophical Transactions of the Royal Society of London A: Mathematical, Physical and Engineering Sciences **361**, 1349 (2003).
[39] We choose the two beams to have equal power, which gives the highest Raman Rabi rate at a fixed total power. Thus, this results in a simple factor of 2 coming from scattering off 2 beams.
[40] R. Wynar, R. S. Freeland, D. J. Han, C. Ryu, and D. J. Heinzen, Science **287**, 1016 (2000).
[41] T. Rom, T. Best, O. Mandel, A. Widera, M. Greiner, T. W. Hänsch, and I. Bloch, Phys. Rev. Lett. **93**, 073002 (2004).
[42] M. Korek, S. Bleik, and A. R. Allouche, J. Chem. Phys. **126**, 124313 (2007).
[43] A. Grochola, P. Kowalczyk, J. Szczepkowski, W. Jastrzebski, A. Wakim, P. Zabawa, and N. P. Bigelow, Phys. Rev. A **84**, 012507 (2011).
[44] J. Zaharova, M. Tamanis, R. Ferber, A. N. Drozdova, E. A. Pazyuk, and A. V. Stolyarov, Phys. Rev. A **79**, 012508 (2009).
[45] A. Grochola, P. Kowalczyk, and W. Jastrzebski, Chemical Physics Letters **497**, 22 (2010).
[46] P. J. Zabawa, *Production of Ultracold, Absolute Vibrational Ground State NaCs Molecules*, Ph.D. thesis, University of Rochester (2012).
[47] L. R. Liu, J. T. Zhang, Y. Yu, N. R. Hutzler, Y. Liu, T. Rosenband, and K.-K. Ni, arXiv:1701.03121 (2017).
[48] There is an additional factor of 2, with both beams at equal power, to account for the Stark shift caused by both beams.
[49] F. H. Mies, E. Tiesinga, and P. S. Julienne, Phys. Rev. A **61**, 022721 (2000).
[50] J. D. Hood, Y. Yu, Y.-W. Lin, J. T. Zhang, K. Wang, L. R. Liu, B. Gao, and K.-K. Ni, Phys. Rev. Research **2**,

023108 (2020).
[51] L. R. Liu, J. D. Hood, Y. Yu, J. T. Zhang, N. R. Hutzler, T. Rosenband, and K.-K. Ni, Science **360**, 900 (2018).
[52] L. R. Liu, J. D. Hood, Y. Yu, J. T. Zhang, K. Wang, Y.-W. Lin, T. Rosenband, and K.-K. Ni, Phys. Rev. X **9**, 021039 (2019).
[53] K. Wang, X. He, R. Guo, P. Xu, C. Sheng, J. Zhuang, Z. Xiong, M. Liu, J. Wang, and M. Zhan, Phys. Rev. A **100**, 063429 (2019).
[54] This interaction shift is larger than the differential axial trapping frequency between Na and Cs atoms, which decouples the relative and center of mass motional state and improves the robustness of our preparation of the relative motional ground state.
[55] M. Endres, H. Bernien, A. Keesling, H. Levine, E. R. Anschuetz, A. Krajenbrink, C. Senko, V. Vuletic, M. Greiner, and M. D. Lukin, Science **354**, 1024 (2016).
[56] D. Barredo, V. Lienhard, S. de Léséleuc, T. Lahaye, and A. Browaeys, Nature **561**, 79 (2018).
[57] A. Cooper, J. P. Covey, I. S. Madjarov, S. G. Porsev, M. S. Safronova, and M. Endres, Phys. Rev. X **8**, 041055 (2018).
[58] D. Ohl de Mello, D. Schäffner, J. Werkmann, T. Preuschoff, L. Kohfahl, M. Schlosser, and G. Birkl, Phys. Rev. Lett. **122**, 203601 (2019).